Article

Oblique-incidence reflectivity difference method combined with deep learning for predicting anisotropy of invisible-bedding shale

Energy Reports

Provided in Cooperation with:
Elsevier

Suggested Citation: Chen, Ru et al. (2020) : Oblique-incidence reflectivity difference method combined with deep learning for predicting anisotropy of invisible-bedding shale, Energy Reports, ISSN 2352-4847, Elsevier, Amsterdam, Vol. 6, pp. 795-801, https://doi.org/10.1016/j.egyr.2020.04.004

Energy Reports 6 (2020) 795–801

Contents lists available at ScienceDirect

Energy Reports

journal homepage: www.elsevier.com/locate/egyr

Research paper

Oblique-incidence reflectivity difference method combined with deep learning for predicting anisotropy of invisible-bedding shale

Ru Chen [a], Zewei Ren [b], Zhaohui Meng [c,d], Honglei Zhan [b,c,*], Xinyang Miao [b], Kun Zhao [c,d,*], Huibin Lü [e], Kuijuan Jin [e], Shijie Hao [d], Wenzheng Yue [a], Guozhen Yang [e]

[a] State Key Laboratory of Petroleum Resources and Prospecting, China University of Petroleum, Beijing 102249, China
[b] Key Laboratory of Oil and Gas Terahertz Spectroscopy and Photoelectric Detection, Petroleum and Chemical Industry Federation, China University of Petroleum, Beijing 102249, China
[c] Beijing Key Laboratory of Optical Detection Technology for Oil and Gas, China University of Petroleum, Beijing 102249, China
[d] Beijing Key Laboratory of Failure, Corrosion, and Protection of Oil/Gas Facilities, China University of Petroleum, Beijing 102249, China
[e] Institute of Physics, Chinese Academy of Sciences, Beijing 100190, China

ARTICLE INFO

Article history:
Received 11 December 2019
Received in revised form 29 March 2020
Accepted 2 April 2020
Available online xxxx

Keywords:
Oblique-incidence reflectivity difference method
Deep learning method
Shale
Anisotropy

ABSTRACT

Deep learning methodologies have revolutionized prediction in many fields and is potential to do the same in the petroleum industry because of the complex oil–gas reservoir. A limitation remains for dense shale exploration in that the shales with invisible bedding are difficult to characterize measurably because of the considerable complexity of the geological structures. The oblique-incidence reflectivity difference method (OIRD) is sensitive to the surface features and was used to obtain a layered distribution of dielectric properties in shales. In this paper, we report a combination of OIRD and deep learning method to identify the dielectric anisotropy of an invisible-bedding shale. The model performs well and clearly identifies the bedding of the shale based on the output values associated with the probability. Only a single direction was determined to have laminations with widths of 20–60 μm. The anisotropy features detected by OIRD also existed in the invisible-bedding shale and were caused by the smaller cracks and denser particles' orientation relative to general shales. As current dense reservoirs include rich invisible-bedding shales, we believe that the OIRD method combined with deep learning method can help improve the exploration efficiency of shale reservoirs.

1. Introduction

Logging observations have found anisotropic layers in the interior of shale reservoirs (Hughes, 2013; Kerr, 2010). The source of shear-wave anisotropy is uncertain, but geophysical models predict large strains along boundaries. It has been suggested that the anisotropy of rock can be divided into types, including the existence of micro-cracks and the orientation of rock particles, which would and would not change the stress, respectively Mashhadian et al. (2018) and Wells et al. (2014). The micro-cracks cause more and larger cracks, thereby creating more fractured channels for hydrocarbon molecules to be extracted (Yang et al., 2017).

The characterization of shale anisotropy is important to the exploration of hydrocarbons (Mokhtari and Tutuncu, 2015). Scanning electron microscopy (SEM) and micro-computer tomography (CT) are employed for microstructure determination, and are thus appropriate for shale detection (Lin and Cerato, 2014; Ma and Chen, 2014). The oblique-incidence reflectivity difference method (OIRD) is sensitive to the dielectric and surface properties of shale because it measures the difference in reflectivity between *s*- and *p*-polarized light (Landry et al., 2006; Liu et al., 2014, 2015). OIRD was employed to measure reservoir rocks and obtain their morphology, the holes' structures, and the adsorption in holes (Zhan et al., 2017a,b; Wang et al., 2016). The anisotropic features of shale and isotropic properties of sandstone have been previously investigated experimentally using OIRD and SEM, but a limitation remains in that the shale used obviously has layers and the lamination direction can be directly identified (Zhan et al., 2016).

In terms of natural geological resources, invisible-bedding shales were found to have large reserves and rich mining value (Chong et al., 2017; Miao et al., 2018). Knowledge of shale with invisible beddings is therefore critical to deciphering reservoir features of shale, which, in turn, can help our understanding of the geophysical properties in the deep Earth (Zhan et al., 2015a; Miao et al., 2016). Precise identification of feature

* Correspondence to: College of New Energy and Materials, China University of Petroleum, 18Fuxue Road, Changping, Beijing.
E-mail addresses: zhanhl@cup.edu.cn (H. Zhan), zhk@cup.edu.cn (K. Zhao).

https://doi.org/10.1016/j.egyr.2020.04.004

anisotropy in invisible-bedding shale is of significance for dense-shale-reservoir exploration. Common methods to characterize anisotropy in shale with invisible bedding include acoustic wave velocity measurement under pressure, ultrasonic wave characterization and seismic response detection. Both the P-wave velocity and the S-wave velocity of the shale show anisotropy in the high-pressure chamber. Young 's modulus and Poisson 's ratio also behave anisotropy (Li et al., 2018; Kuila et al., 2011). In ultrasonic testing, the ultrasonic wave speed and waveform will change due to changes in the internal structure of the shale. The relationship between wave velocity and anisotropy of shale media can be described by petrophysical models (Zhubayev et al., 2016). In seismic response detection, seismic wave velocity has strong dispersion and attenuation in viscoelastic media. The anisotropic response of reservoir azimuth varies with fracture parameters and shows different characteristics (Wang, 2002). Compared with these conventional methods, OIRD measurement causes none damage to the original shale samples, requires little preliminary preparation and has a simple test condition.

The success of supervised deep learning models, especially convolutional neural networks (ConvNets or CNNs), have fueled research into their application in various fields. The ConvNet models have been successfully applied in the computer vision field such as handwritten digit recognition and image classification. And in the field of identifying and processing images obtained by optical devices, deep learning algorithms have powerful capabilities and enormous potential (Washburn et al., 0000). As another example of the potential of deep learning in shale anisotropy research, this paper introduces the application of the ConvNet model in the OIRD image data set.

In the work reported in this paper, we applied the OIRD method to quantify the surface properties of subsurface shale on the basis of an obscure measurement by SEM. To reveal the anisotropy information and the lamination properties of the shale, a principal component analysis (PCA) method was used on the basis of OIRD signal intensities. The results suggest that OIRD combined with statistical methods can be used for shale-core analysis with invisible laminations, indicating that there would be a new selection for super-dense-shale-reservoir exploration.

2. Experimental methods

Sample preparation. Shale rock without visible anisotropy was cored in the horizontal direction. The petrophysical layers are perpendicular to the upper and lower surface of the core. The shale core is a cylinder measuring 25 mm in diameter and 50 mm in length. To obtain the parallelism of shale surfaces, the shale core was cut and then polished before all measurements. Generally, shale has a vectored stratification plane over the entire space, while the bedding of the shale used in this experiment is invisible. The bedding direction cannot be directly confirmed before each measurement.

Direct OIRD scanning. Fig. 1 is a schematic of the OIRD experimental setup for the detection of shale core. The optical beam is a He–Ne laser with wavelength of $\lambda = 632.8$ nm. It initially passes through a polarizer (P) to ensure p-polarized incidence. The polarization of the laser between *p*- and *s*-polarization is oscillated by a photoelastic modulator (PEM) at a frequency of 50 kHz. The laser then enters a phase shifter (PS) to create a fixed phase difference Φ_{ps} between the *p*- and *s*-polarization components. The laser reflected from the sample is introduced into a polarization analyzer (PA) with the transmission axis set from s-polarization. The intensity can be detected by a silicon photodiode (PD). We use two lock-in amplifiers to measure the first harmonic $I(1\ \Omega)$ and second harmonic $I(2\ \Omega)$ signals. Finally, the $I(2\ \Omega)$ and $I(1\ \Omega)$ signals of $Im\{\Delta p - \Delta s\}$ and $\mathrm{Re}\{\Delta p - \Delta s\}$ are recorded by a computer. The $I(2\ \Omega)$ and $I(1\ \Omega)$ signals include information about the surface and the dielectric properties of the sample. In terms of OIRD detection, no special requirements with respect to the samples were needed, and they can be fastened onto the upper surface of the stage. The OIRD instrument uses a stepper motor to move the sample and the frequency of the collected signal to be scanned can be adjusted, thus kinds of rock samples can be measured by increasing the frequency of the collected signal and the moving speed of the motor when scanning a large sample. OIRD is not only sensitive to the surface features of the shale with much anisotropy information, but also helpful to scan large surface for identification of the geological structures. The scanning parameters can be changed depending on the scanning area. Generally, it will take half an hour to scan 5 cm × 5 cm shale by OIRD. The measurements were performed under ambient conditions. The interval between two adjacent scans can be 1 μm. In the experiment, the scanning step length was 4 μm. In this research, $Im\{\Delta p - \Delta s\}$ was used as the parameter to detect the shale surface.

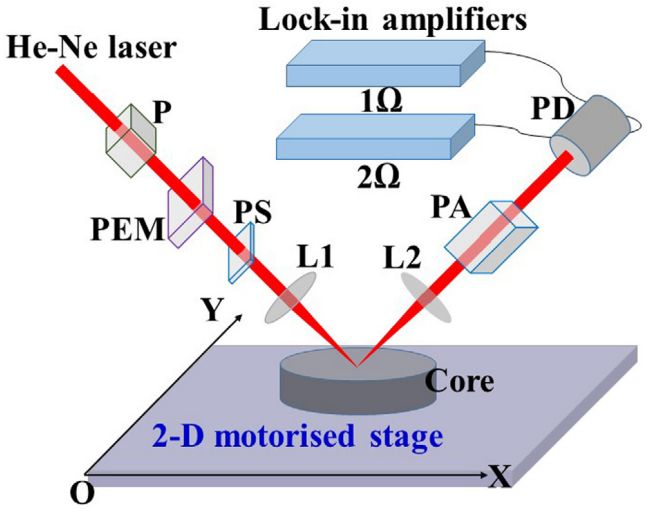

Fig. 1. Schematic picture of the OIRD experimental setup.

Deep learning model architecture. Since convolutional neural network architectures are good at spatially-correlated feature extraction, a convolutional model was designed for dielectric anisotropy of invisible-bedding shale probed. Fig. 2 showed the architecture of the deep learning model. The surface of the shale with obvious bedding was scanned by OIRD, and the data obtained was used as input data directly without conversion to images. These data were split into several subsets of 50*250, and the data obtained by the horizontal and vertical cuts ware labeled 1 and 0, respectively. Then, 80% of the segmented data was divided into training sets, 20% was divided into verification sets, and there was no intersection between the two subsets. In a convolutional layer, the features are extracted from the input by sliding filters with convolution operations, generating feature maps correspondingly. The model consists of 12 convolutional layers with strides of 1 and kernel sizes of 3 × 3, where the feature depth gradually increases from 16 to 64 output channels. Between the convolutional layers, down-sampling was performed by three max pooling layers with a 2 × 2 window size. The output of the last convolutional layer was flattened to one-dimensional data and then regularized (regularization parameter was 0.0001). Then three fully-connected layers were attached immediately after each one have 128 nodes, and dropout regularization was applied to them; the third one produces the unnormalized logits for the two categories to be classified. Finally, the predicted

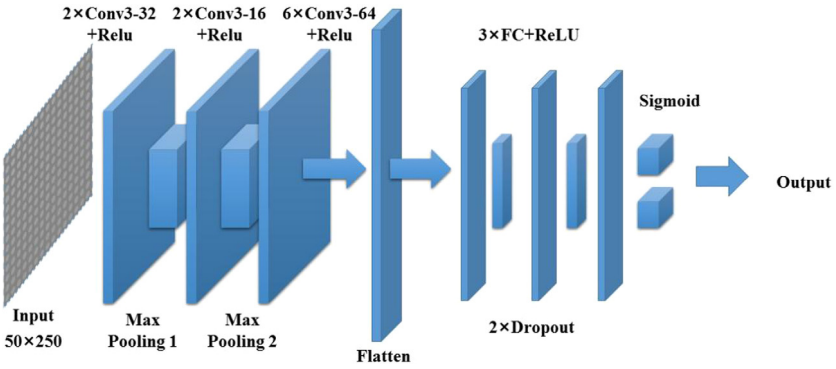

Fig. 2. The architecture of the deep learning model. The deep convolutional neural network model (inspired by VGGNet) consists of 10 convolutional layers, 2 maximum pooling layers, and 3 fully connected layers. The convolutional layer extracts and learns features of an input example with a 3 × 3 kernel (m × Conv3-p ReLU represents m convolutional layers with p output filters and ReLU activation functions). The first two fully connected layers have full connectivity to all nodes in the previous layer, and discard regularization is applied after them. The probabilities of these two categories are output on the sigmod layer and the input examples are classified.

probabilities of the classes are obtained by a Sigmoid layer from the logits. By using these probabilities, the cross-entropy error can be calculated and minimized by the Adam optimizer during back propagation and the variables of the model are updated iteratively. To introduce nonlinearity, all convolutional and fully-connected hidden layers are equipped with Rectifed Linear Unit (ReLU). After the data was substituted into the established model, the output data related to the predicted probability value could be obtained. Meanwhile, the total time of 80 epochs was less than 10 min because the scanning imaging results of OIRD will obtain data in text format. These data are cut into pieces with 50 × 250 size in advance, witch further saves the calculation amount. The neural network structure applied in this study has been optimized. Therefore, the calculation process will be greatly simplified compared with traditional image recognition.

Principal component analysis. PCA is a mathematical method used to reduce the number of dimensions within the data while retaining as much of the overall variation as possible based on uncorrelated projections (Zhan et al., 2015b). The OIRD data are set as the input of matrix as follows:

$$X = \begin{bmatrix} x_{11} & x_{12} & \cdots & x_{1n} \\ x_{21} & x_{22} & \cdots & x_{2n} \\ \vdots & \vdots & \ddots & \\ x_{m1} & x_{m2} & \cdots & x_{mn} \end{bmatrix},$$

where m and n are the number of samples and number of sample dimensions, respectively. A linear transformation of X will be calculated and Y is obtained as follows:

$$\begin{cases} Y_1 = u_{11}X_1 + u_{12}X_2 + \cdots + u_{1n}X_n \\ Y_2 = u_{21}X_1 + u_{22}X_2 + \cdots + u_{2n}X_n \\ Y_n = u_{n1}X_1 + u_{n2}X_2 + \cdots + u_{nn}X_n \end{cases}.$$

There is no correlation between Y_i and Y_j $(i \neq j, i, j \in (1, n))$. Meanwhile, Y_1 is the linear combination with the largest variance and is described as the first principal component (PC 1). Similarly, Y_2 is the linear combination that is not related to Y_1 and is called PC 2. Analogous to this, Y_n is the last PC with the smallest variance. A basic limitation of the linear combination is $u_{k1}^2 + u_{k2}^2 + \cdots + u_{kn}^2 = 1, k = 1, 2, \ldots, n$.

Ultrasonic measurement. Longitudinal waves (P waves), an important branch in bulk waves, is the first significant peak, which has often been employed for detecting thickness, density, and elasticity (Lu et al., 2015). A high-energy pulsed laser (20 mJ/pulse) emits the shale core and excites ultrasonic waves via thermoelastic expansion, which can be measured by a laser ultrasonic receiver. The adaptive laser interferometer is a specific type of interference receiver. The receiver uses two-wave mixing in a photorefractive crystal to deliver the displacement of the sample and has a sensitivity with a bandwidth from 10 kHz to 10 MHz. The shale core is placed directly on the rotating table for rotational measurement. The ultrasonic longitudinal waves are then measured at intervals of 5° until the rotation is returned to the test starting point.

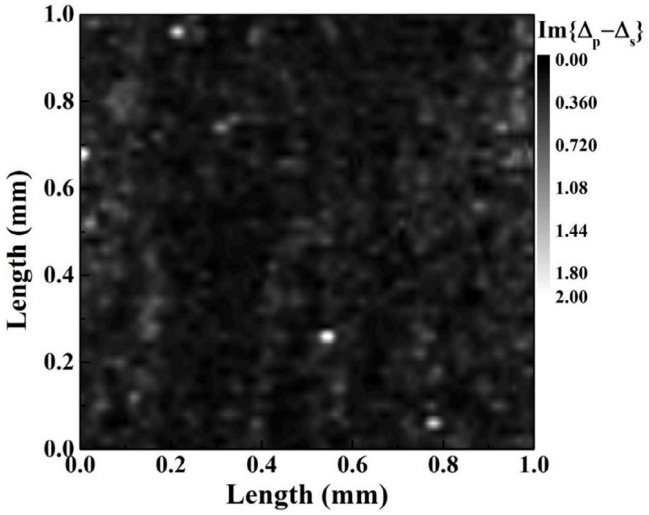

Fig. 3. 2D image of OIRD $Im\{\Delta_P - \Delta_S\}$ of shale core.

3. Analyses and results

A basic investigation was initially performed into the anisotropy of shale. The typical types of the anisotropy of shale include the existence of micro-cracks and their arrangements in different directions, as well as the orientation of the mineral particles. Generally, the layered structure of shale is detected by SEM. However, some shale reservoirs exhibit non-obvious anisotropy, which is difficult and necessary to detect. OIRD method is thus introduced to identify the anisotropy of shale.

The shale core, without obvious lamination or a layered structure, was then analyzed using the OIRD system. The sample was placed on a 2D stage and the phase shifter as well as polarization analyzer were adjusted to make the signals $I(2\ \Omega)$ and $I(\Omega)$ equal to zero. The shale core was then scanned in a random region measuring 1 mm×1 mm. The real signal $Re\{\Delta_P - \Delta_S\}$,

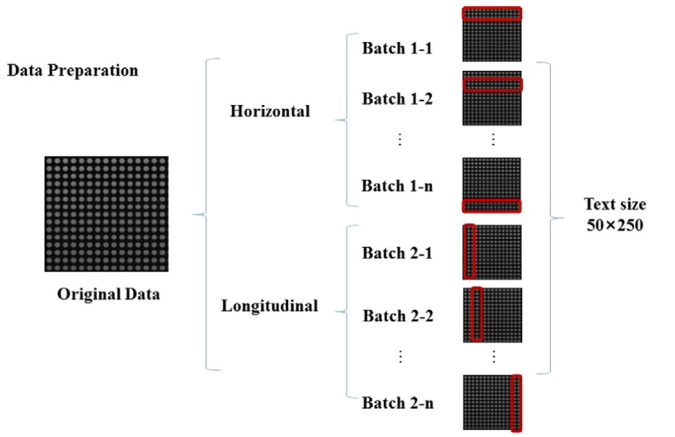

Fig. 4. The schematic picture of data preparation and deep learning calculation.

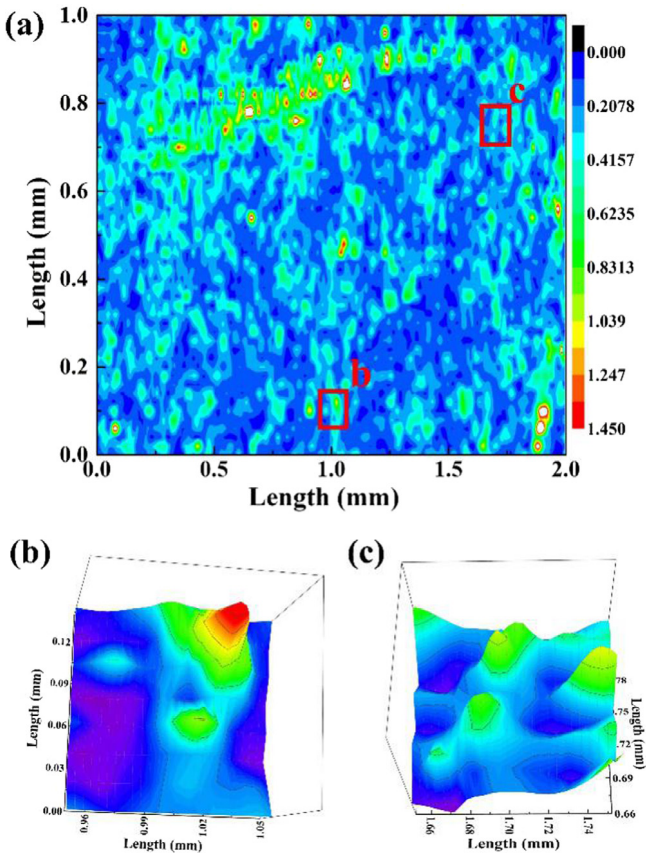

Fig. 5. The calculated OIRD image for the invisible-bedding shale based on the deep learning network. (a) A two-dimensional image of the output data associated with the probability value. A number of stripes were obtained parallel to the 1 mm side and perpendicular to the 2 mm side. (b) A 3D image of the output data of the selected region b. (c) A 3D image of the output data of the selected region c.

imaginary signals Im$\{\Delta_P - \Delta_S\}$, and their relative coordinates were recorded by a computer. Fig. 3 is the intensity profile taken along a rectangular area showing the signal images of Im$\{\Delta_P - \Delta_S\}$ obtained from the shale core. Im$\{\Delta_P - \Delta_S\}$ is altered with changing scanning position, which revealed the variance of dielectric properties depending on the positions of the shale-core surface. Some maximum and minimum signals can be observed and the respective peaks are located at different points. Fluctuations are also observed in some areas, indicating that the dielectric information of the sample surfaces are reflected in the OIRD signals.

On the whole, the layered structure and anisotropy property of invisible-bedding shale are hard to be directly detected. Deep learning method, which is useful for revealing the rich information in the data, was employed to calculate the OIRD imaging data. Fig. 4 shows the data preparation and deep learning calculation. The OIRD scan data file is used directly as input data without conversion to an image. Originally, these waveform elements were two-dimensional spatial sequence data. In order to adapt to the conventional convolutional neural network architecture, these elements are divided into several 50 × 250 two-dimensional data according to the difference between the horizontal and vertical selection methods. The entire data set is divided into three subsets, including training, validation, and test data sets.

Fig. 5(a) shows the output image associated with the probability value obtain image classification after the Re$\{\Delta p - \Delta s\}$ signal obtained by the shale core is substituted into the deep learning neural network. The output signal strength differences show the change in the dielectric properties of the shale core surface as a function of position. Multiple stripes are parallel to the 1 mm side and perpendicular to the 2 mm side. The width of the secondary laminate was found to range from a few microns to tens of microns. Figs. 5(b) and (c) show 3-D images of two randomly selected regions in the output data. The resolution of the image is significantly improved compared to the experimental results of shale anisotropy in Fig. 3. In these figures, two or three beddings can be clearly seen. In these two regions, the width of the peak area and the distance between the continuous peaks are 5–30 μm, which is consistent with the actual stratification of the shale. Therefore, this deep learning model based on convolutional neural networks can be used to identify OIRD image data of shale containing bedding.

4. Discussion

The layered structures of invisible-bedding shale is clearly reflected by the OIRD image combined with deep learning calculation. In order to detect the structural information and validate the results obtained by deep learning, SEM, PCA and laser ultrasonic measurements were performed to analyze the shale scanned by OIRD. SEM was initially employed to analyze invisible-bedding shale, shown in Fig. 6. Obvious cracks and orientations of rock can be barely observed throughout the measured areas.

A PCA method was used on the basis of OIRD signal intensities. According to the characteristics of OIRD scanning, the 2D signal data were divided into two types: one based on the vertical direction as the variance and every horizontal line as a group and the other related to the horizontal direction as the variance and every vertical direction as a group. In the PCA calculation, PC 1, whose variance was maximized, reflected most information according to the largest contribution rate that can be used to describe the importance of PCs to the samples. PC 2 reflected the second-largest amount of information. Herein, the first two PCs of the OIRD data set are found to describe more than 90% of the variance within the data. Owing to its large contribution, PC 1 is of great importance to the analysis of the dielectric properties. Fig. 7(a) shows the vertical length dependence of the PC 1 and PC 2 scores obtained from the OIRD signal data in Fig. 3. Both PC 1 and PC 2 scores are altered from −1.0 to 1.5 over the entire vertical length range, and the average PC 1 as well as PC 2 scores are equal to approximately zero. None of the PC peaks can be observed. Consequently, PC 1 and PC 2, which were obtained on the basis of the OIRD signal, are basically unchanged at all the locations in the vertical direction, indicating that the dielectric properties remained uniform.

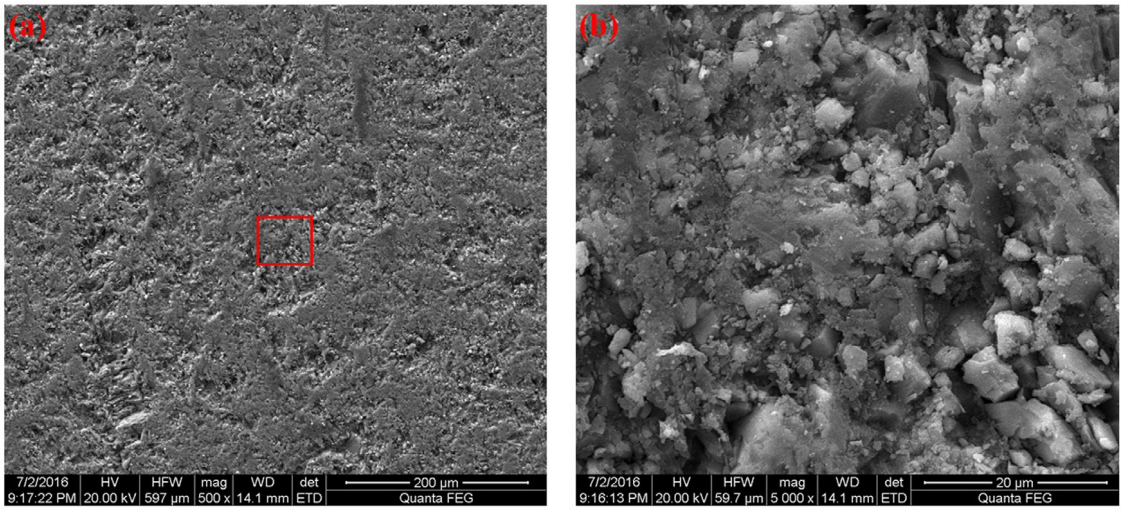

Fig. 6. SEM images of shale core measured by OIRD system.

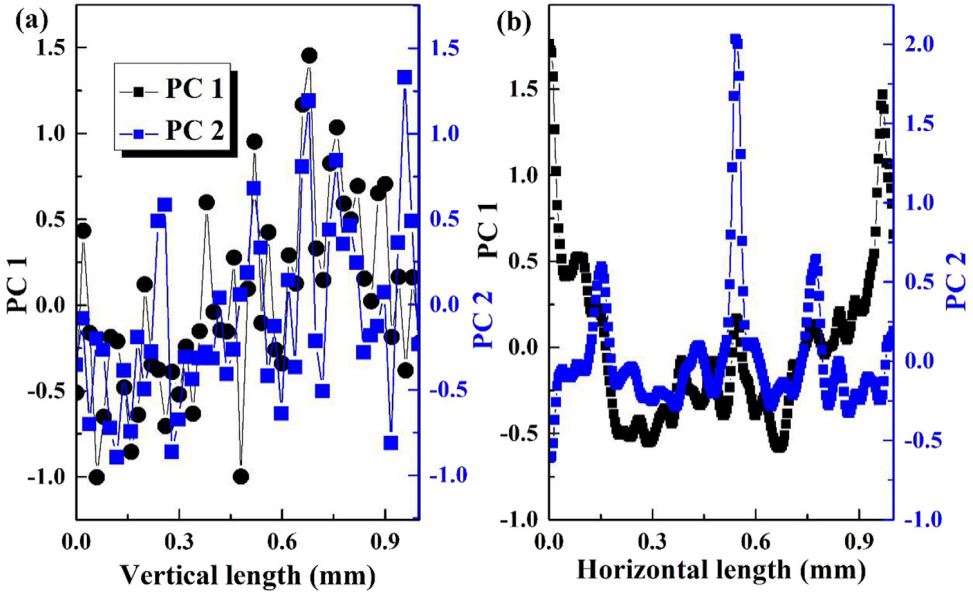

Fig. 7. PCA based on the OIRD scanning image. (a) PC 1 and PC 2 vs vertical length of OIRD scanning area. (b) PC 1 and PC 2 vs horizontal length of OIRD scanning area.

Meanwhile, we performed a further calculation of the OIRD signal data in the horizontal direction using a PCA algorithm. As shown in Fig. 7(b), the PC intensities are different at different positions, revealing the position-dependent variance of the OIRD signal properties on the shale-core surface. PC 1 represents the major information of OIRD signal distribution caused by the shale. A number of peaks were obtained and were parallel to the vertical side and perpendicular to the horizontal side. The results showed that the shale has the adjacent laminations with the width of ∼100–300 μm because of the first-class features located at the positions of 0.084, 0.384, 0.544, 0.768 and 0.968 mm. The secondary laminations were hardly detected by PCA. Consequently, the shale has the bedding structure in a single direction.

Shales are often anisotropic owing to the combined effect of partial alignment of platy clay particles, layering and kerogen inclusions. In order to detect the distribution features of similar components, ultrasonic measurement was employed herein. It is a general way of determining the isotropic features in rock that proved that the elastic properties are isotropic in the directions parallel to the bedding, while they are anisotropic in other directions. To confirm the directional properties in the inner shale, ultrasonic measurement was employed to scan a 360°-circle curve. Fig. 8(a) shows the ultrasonic measurement of the shale, by which the travel-time map of the shale can be obtained at different θ values. The time–voltage curves can reveal a peak-picking program located at the time of the first peak. On the basis of the travel time τ_1, the propagation speeds v were calculated for the shale at different θ values. Fig. 8(b) plots the angle-dependent longitudinal wave velocity of the shale. It is clear that the velocity ranges from ∼3200 to 3800 m/s and that the shale has a significant anisotropy of velocity with the data symmetry at the location of 180°. According to the velocity curve in Fig. 8(b), there are three maximum data at the degrees of 0°, 180°, and 360° and two minimum data at the degrees of 90° and 270°. In the ranges from 0° to 90° and from 180° to 270°, the velocity decreases gradually with increasing θ; in contrast, in the ranges from 0° to 90° and from 180° to 270°, the velocity decreases gradually with increasing θ. These results reveal the propagation of longitudinal waves reaching a maximum along the bedding

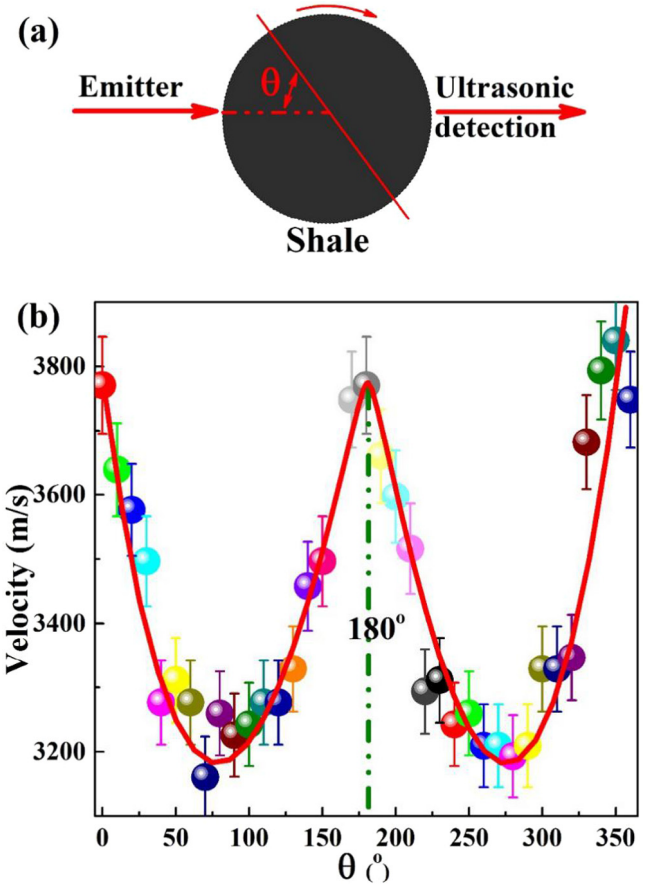

Fig. 8. Ultrasonic analysis of shale measured by OIRD and SEM. (a) Schematic of shale sample for input laser. Assuming that there exists a fixed direction of bedding in the shale, a θ degree can be obtained between the direction of the laser and that of the bedding. (b) θ-dependent longitudinal wave velocity. Error bars represent a $\pm 5\%$ fluctuation of relative deviation.

surface of the shale and a minimum along the surface vertical to the beddings in the shale.

The schematic illustration of the resistance measurements was presented in Fig. 9(a). The resistance of shale was tested with the ohm of multimeter and the two electrodes were always kept 1 cm. The parameter θ from 0 to 360° is the angle between the direction of electric field in the first test and the later test. As shown in Fig. 9(b), the resistance of shale is in MΩ grade. The shale has a significant anisotropy, and there is a symmetry at the location where the θ is 180°. The maximum resistance of 27 MΩ is obtained at the direction of electric field. This direction is perpendicular to the direction of shale. The minimum of 8 MΩ was also observed. The periodic changes of θ-R curves predicted the bedding shale of shale. Similar to the ultrasonic analysis, resistance measurement can detect the bedding direction, while it can hardly provide more information such as the shale structure. OIRD and deep learning can provide a supplementary analysis.

Therefore, OIRD combined with deep learning calculation predicted the anisotropy of the invisible-bedding shale. Deep learning approaches such as CNNs are largely responsible for a recent paradigm shift image and natural language processing. Compared with traditional machine learning algorithms, deep learning emphasizes learning from massive data, and solves the problems that traditional machine learning algorithms such as high-dimensional, redundant, and high-noise existing in massive data are difficult to handle. Specifically, the stratification of shale in this paper is reflected in the numerical fluctuations of the OIRD scan data. Through supervised learning, the layered rationality of shale in the data has been extracted by the neural network and stored in the model in the form of weight values. The features in the image data obtained by the OIRD scan are well extracted by the convolution operation. Based on the results in this research, OIRD combined with deep learning is a very promising and practical technology for detect the shale reservoir, which is very useful for the conventional techniques in this field.

5. Conclusions

This research focused on using a new combination of OIRD and deep learning in the investigation of the anisotropy in invisible-bedding shale. Invisible-bedding shale was found to have laminations with widths of 20–60 μm. The shale had the bedding structure in a single direction, which can hardly be characterized with a single conventional method. The anisotropy of dense shale influences many aspects of exploration owing to the different strength properties of the stratification layers in shale. Consequently, OIRD combined with deep learning supply a very promising technology for detecting the anisotropy in dense shales.

Declaration of competing interest

The authors declare that they have no known competing financial interests or personal relationships that could have appeared to influence the work reported in this paper.

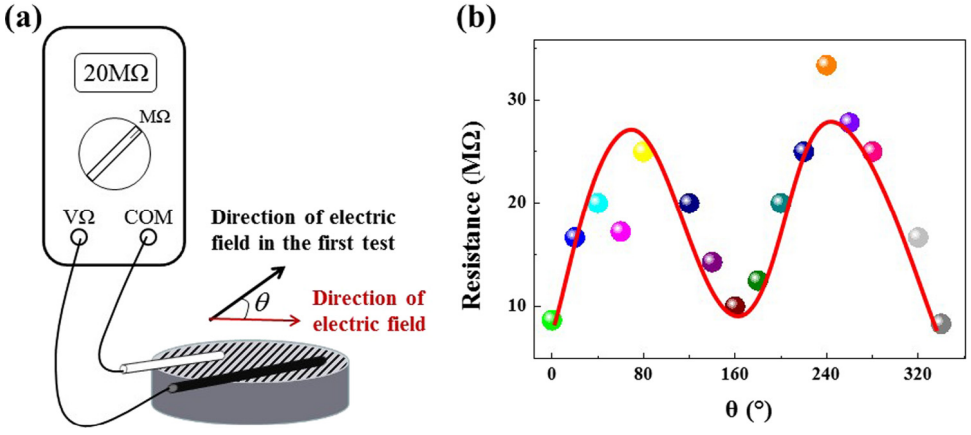

Fig. 9. (a) Experimental device diagram; (b) Angle dependent measured (dots) and fitted resistance (dotted curve) of the shale sample between 0°–360°.

CRediT authorship contribution statement

Ru Chen: Methodology, Writing - original draft. **Zewei Ren:** Data curation. **Zhaohui Meng:** Validation. **Honglei Zhan:** Conceptualization, Writing - review & editing. **Xinyang Miao:** Supervision. **Kun Zhao:** Writing - review & editing. **Huibin Lű:** Data curation. **Kuijuan Jin:** Data curation. **Shijie Hao:** Visualization, Investigation. **Wenzheng Yue:** Software, Validation. **Guozhen Yang:** Writing - review & editing.

Acknowledgments

We thank the National Nature Science Foundation of China (Grant No. 11804392), the Science Foundation of China University of Petroleum, Beijing, China (NOs. 2462017YJRC029, ZX20190163 and 2462018BJC005) and the University-Industry Collaborative Education Program (No. 201901066031) for the financial support. We would like to thank LetPub (www.letpub.com) for providing linguistic assistance during the preparation of this manuscript.

References

Chong, Z., et al., 2017. Numerical investigation of bedding plane parameters of transversely isotropic shale. Rock Mech. Rock Eng. 50, 1–22.
Hughes, J.D., 2013. Energy: A reality check on the shale revolution. Nature 494, 307–308.
Kerr, R.A., 2010. Natural gas from shale bursts onto the scene. Science 328, 1624–1626.
Kuila, U., et al., 2011. Stress anisotropy and velocity anisotropy in low porosity shale. Tectonophysics 503 (1–2), 34–44.
Landry, J.P., et al., 2006. Incidence-angle dependence of optical reflectivity difference from an ultrathin film on a solid surface. Opt. Lett. 31, 531–533.
Li, Xiaying, et al., 2018. Response of velocity anisotropy of shale under isotropic and anisotropic stressfields. Rock Mech. Rock Eng. 51, 695–711.
Lin, B.T., Cerato, A.B., 2014. Application of SEM and ESEM in microstructural investigation of shale-weathered expansive soils along swelling-shrinkage cycles. Eng. Geol. 177, 66–74.
Liu, S., et al., 2014. Label-free, real-time detection of the dynamic processes of protein degradation using oblique-incidence reflectivity difference method. Appl. Phys. Lett. 104, 163701.
Liu, S., et al., 2015. Characterization of monoclonal antibody's binding kinetics using oblique-incidence reflectivity difference approach. mAbs 7, 110–119.
Lu, Z.Q., et al., 2015. Non-contact measurement of the water content in crude oil with all-optical detection. Energy Fuels 29, 2919–2922.
Ma, T., Chen, P., 2014. Study of meso-damage characteristics of shale hydration based on CT scanning technology. Petrol. Explor. Dev. 41, 249–256.
Mashhadian, M., et al., 2018. Assessing mechanical properties of organic matter in shales: Results from coupled nanoindentation/SEM-EDX and micromechanical modeling. J. Petrol. Sci. Eng. 165, 313–324.
Miao, X.Y., et al., 2016. Oil yield characterization by anisotropy in optical parameters of the oil shale. Energy Fuels 30, 10365–10370.
Miao, X.Y., et al., 2018. Ultraviolet laser-induced voltage in anisotropic shale. J. Phys. D: Appl. Phys. 51, 045503.
Mokhtari, M., Tutuncu, A.N., 2015. Characterization of anisotropy in the permeability of organic-rich shales. J. Petrol. Sci. Eng. 133, 496–506.
Wang, Z.J., 2002. Seismic anisotropy in sedimentary rocks, part 2: laboratory data. Geophysics 67 (5), 1423–1440.
Wang, J., et al., 2016. Evaluation of simulated reservoirs by using the oblique-incidence reflectivity difference technique. Sci. China Phys. Mech. Astron. 59, 114221.
Washburn, J.D., et al., Evolutionarily informed deep learning methods for predicting relative transcript abundance rom DNA sequency, PNAS 116, 5542–5549.
Wells, R.K., et al., 2014. Microstructures and rheology of a calcite-shale thrust fault. J. Struct. Geol. 65, 69–81.
Yang, J., et al., 2017. Nanoscale geochemical and geomechanical characterization of organic matter in shale. Nature Commun. 8, 2179.
Zhan, H.L., et al., 2015a. Qualitative identification of crude oils from different oil fields using terahertz time-domain spectroscopy. Fuel 143, 189–193.
Zhan, H.L., et al., 2015b. Spectral characterization of the key parameters and elements in coal using terahertz spectroscopy. Energy 93, 1140–1145.
Zhan, H.L., et al., 2016. Real-time detection of dielectric anisotropy or isotropy in unconventional oil-gas reservoir rocks supported by the oblique-incidence reflectivity difference technique. Sci. Rep. 6, 39306.
Zhan, H.L., et al., 2017a. In situ monitoring of water adsorption in active carbon using an oblique-incidence optical reflectance difference method. AIP Adv. 7, 095219.
Zhan, H.L., et al., 2017b. Oblique-incidence reflectivity difference application for morphology detection. Appl. Opt. 56, 8348–8352.
Zhubayev, A., et al., 2016. Ultrasonic velocity and attenuation anisotropy of shales, Whitby, United Kingdom. Geophysics 81 (1), D45–D56.